JOURNAL OF CELLULAR PLASTICS

*Article*

Journal of Cellular Plastics
48(2) 141–159

DOI: 10.1177/0021955X11432970
cel.sagepub.com
SAGE

# Supercritical $CO_2$ in injection molding can produce open porous polyurethane scaffolds – a parameter study

**Hong-Bin Wu[1], Håvard J Haugen[2] and Erich Wintermantel[1]**

## Abstract

There are several methods of producing open porous polymer structures for medical use. However, very few are applicable to industries and are therefore limited to both number of samples and batch variations. This study presents an industrial microcellular injection molding process, known as MuCell® technology, which was used to produce highly porous scaffolds of thermoplastic polyurethane. A parameter study was performed to quantify and analyze the effect of the processing parameters on the porous structure. Six key parameters (gas content, weight reduction, injection speed, mold temperature, plasticizing pressure, and temperature) were tested with an iteration method. The pore structure was determined with advanced micro Computer Tomography algorithm. All key processing parameters were identified. Gas content and weight reduction showed a more profound effect on the pore morphology than other parameters on the pore structure. It was possible to produce scaffolds with open porosity as high as 71%. The study concludes that MuCell® technology is an accurate and liable production method for large-scale production of open porous thermoplastic polyurethane scaffolds, and supercritical fluid could, therefore, be a potential production method for polymer scaffolds.

[1]Department and Chair for Medical Engineering, Technische Universität München, Boltzmannstr. 15, D-85748 Garching, Germany.
[2]Department of Biomaterials, Institute for Clinical Dentistry, University of Oslo, PO Box 1109, Blindern, NO-0317 Oslo, Norway.

**Corresponding author:**
Håvard J Haugen, Department of Biomaterials, Institute for Clinical Dentistry, University of Oslo, PO Box 1109, Blindern, NO-0317 Oslo, Norway
Email: h.j.haugen@odont.uio.no

**Keywords**
MuCell®, injection molding, pore structure, thermoplastic polyurethane, scaffold, microCT, open porous, gas content, polyurethane foams, cell density, cell growth, gas injection, supercritical fluid

## Introduction

Cells are often implanted or 'seeded' into an artificial structure that is capable of supporting three-dimensional (3-D) tissue formation.[1,2] These structures are typically called scaffolds. Polymer scaffolds are widely used in different tissue engineering applications[3–9] and are often critical, both *ex vivo* as well as *in vivo*, to recapitulate the *in vivo* milieu and allow cells to influence their own microenvironments. Scaffolds usually serve at least one of the following purposes: (1) allow cell attachment and migration, (2) deliver and retain cells and biochemical factors, (3) enable diffusion of vital cell nutrients and expressed products, and (4) exert certain mechanical and biological influences to modify the behavior of the cell phase.[10,11] Porous polymer like polyurethane has been suggested for different uses, such as orthopaedic,[12] neo-meniscal tissue,[6] and bone tissue engineering.[13–16] At present, various techniques are used to produce a scaffold with a microcellular structure, such as thermally induced phase separation, solvent casting/particle leaching, electro-spinning, etc.;[17–19] however, very few are applicable to industries for producing large number of samples at a low cost.[20–22] Batch variations could also be a problem. Turng and Kramschuster[23] utilized supercritical fluid within injection molding and particulate leaching techniques to produce highly porous and interconnected structures of polylactide and polyvinyl alcohol). The only work on industry-applicable processing methods for polyurethanes is by Leicher et al.,[24] which was the initiator for this study.

In this study, an industrial microcellular injection foaming process, known as MuCell® technology, was chosen to produce a scaffold with an open porous structure. An industry-applicable processing method such as the MuCell® was preferred due to its large capacity and high accuracy. MuCell® technology is a polymer process method that is normally used in automobile and furniture industries.[25–28] It uses supercritical $CO_2$ as a blowing agent, which is injected into the plasticization section of the injection molding machine (Figure 1). The blowing agent is injected into the polymer melt through the gas supply line and injector, in its supercritical state, by the plasticization phase of the injection molding machine. After plasticization, the mixture of polymer melt and gas is injected through the nozzle into the mold, where the foam structure can be generated due to the quick pressure drop in the mold. The main products which are produced today using MuCell® technology have closed cellular foam in order to reduce weight, but they retain the mechanical properties.[29–31] Closed pore structure is of no use in tissue engineering applications, as cell and tissue need entrances to the pore structure. In addition, transfer of nutrients and waste products are only possible with an open porous structure.[32,33]

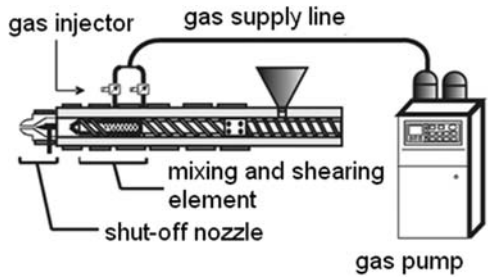


**Figure 1.** Draft of the MuCell® technology (figure according to Wintermantel and Ha[34]).

This study aims to utilize the MuCell® technology to produce an open porous polyurethane structure to identify the key processing parameters and try to quantify the main processing parameters which govern the open pore structure and morphology. The choice of changeable parameters was made based on the simulation models from nucleation theory and literature search.[24,35,36] The experiments were done by varying one of variable parameters while keeping the others constant. Medical grade thermoplastic polyurethane (TPU; Texin® 985, Bayer, PA, USA) was chosen as the raw material for the scaffold due to its excellent mechanical properties, biocompatibility, and biostability.[37–40] The biocompatibility of the scaffolds was, due to scope of this study, not tested here and will be published separately.

## Materials and methods

### *Polymer processing*

Medical grade non-degradable TPU (Texin® 985, Bayer, PA, USA) was used as the raw material. An injection molding machine (KM 125-520C2, KraussMaffei Technologies GmbH, Munich, Germany) with a temperature control unit for cooling the mold (90S/6/TS22/1 K/RT45, Regloplas, St. Gallen, Switzerland) was used for the production of the samples. The injection molding machine was equipped with a MuCell® package by the Trexel Inc., Woburn, MA, USA. $CO_2$ was used as the blowing agent ($CO_2$ protective gas DIN-32525-C1, Westfalen AG, Münster, Germany). The used mold was capable of producing six ring-shaped scaffolds with a diameter 32 mm and thickness 11 mm in one cycle.

### *Experimental strategy*

The investigated parameters and range was found from the nucleation theory.[41,42] Figure 2 shows the main governing factors for the formation of porous polymers.[35] Level I indicates the first prime factors that directly affect cell nucleation and growth and level II the second ones which influence the first factors and also

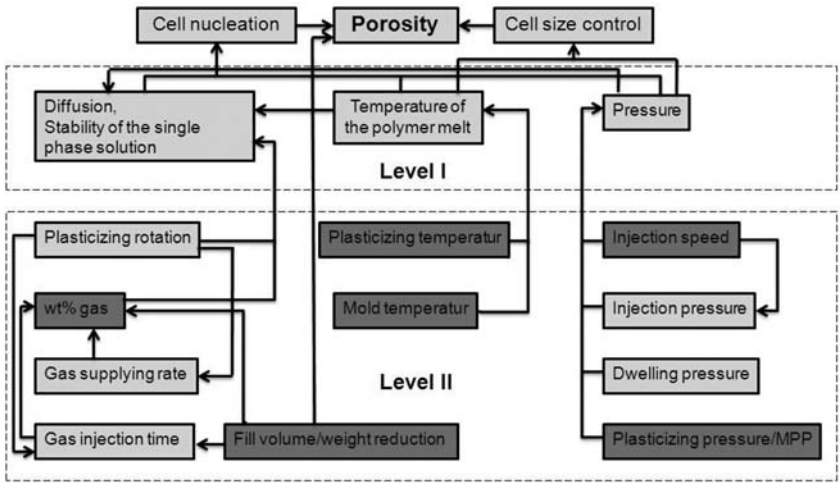


**Figure 2.** Classification and selection of process controlling parameters for cell nucleation and growth.

adjustable in the MuCell® process. The factors indicated on a dark background are those which were investigated in this study. The choice of the changeable parameters was made based on the knowledge given by nucleation theory and literature search.[35,36] The ranges of variable parameters and the values of fixed parameters are presented in Table 1. The experiments were done by varying one of the variable parameters while keeping the others constant.

## *Characterization of macro- and microstructures*

Scanning electron microscopy (SEM; Jeol JSM-6060LV, JEOL Ltd, Tokyo, Japan) was used for the observation of pore morphology of the cross-section of the scaffold. The samples were sliced with a scalpel and then coated with a thin layer of gold using a sputter-coater (SCD 005, BAL-TEC AG, Balzers, Lichtenstein) under high vacuum with a current range between 5 and 15 kV. Characteristics of the porous structure such as pore size and porosity can be calculated by counting the average cell number and size of several SEM images from one sample.

MicroCT (SkyScan 1172, SkyScan, Kontich, Belgium) was used to quantitatively measure the porous interconnectivity of scaffolds: three $8 \times 11\,mm^2$ cylindrical samples from each scaffold ($n = 3$) at 7 μm resolution using a voltage of 59 kV and a current 167 μA. Samples were rotated 180° around their long axis and three absorption images were recorded every 0.400° of rotation.

The image analysis of the reconstructed axial bitmap images was performed using the standard SkyScan software (CTan, SkyScan, Kontich, Belgium). The threshold value was set between 65 and 225 for this study. Additional noise was removed by the 'despeckling' function. All objects smaller than 500 voxels and not

**Table 1.** Ranges of variable parameters and values of fixed parameters of the MuCell® process in this study

| Variable parameters | Examined range |
|---|---|
| $CO_2$ concentration | 1–6% wt |
| Degree of weight reduction | 35–65% |
| Injection speed | 30–300 mm/s |
| Plasticizing pressure/microcellular process pressure (MPP) | 160–220 bar |
| Plasticizing temperature | 180–210°C |
| Mold temperature | 25–85°C |
| Fixed parameters | Value |
| Cooling time | 120 s |
| Dwell pressure | 450 bar |
| Beginning dwell pressure | 0.5 mm |
| Duration of dwell pressure | 0.5 s |
| Clamp tonnage | 200 kN |
| Plasticizing rotation | 40 per min |
| Injection pressure | 0–3000 bar |

Notes: The MPP was an active pressure that keeps the gas in the polymer melt. This pressure was actually the plasticizing pressure.

connected to the 3-D body were thus removed prior to further analysis. In order to eliminate the potential edge effects, a cylindrical volume of interest (VOI) with a diameter 5 mm and height 2.5 mm was selected in the center of the scaffold. Scaffold porosity was then calculated as follows:

$$\text{Porosity} = 100\ \% - \text{vol. \% of binarized object (scaffold materials) in VOI} \quad (1)$$

All images underwent 3-D analysis, followed by the quantification of interconnectivity using the advanced 'shrink-wrap' function, which allows to measure the interconnectivity.[43] A shrink–wrap process was performed between two 3-D measurements to shrink the outside boundary of the VOI in a scaffold through any openings, the size of which was equal to or larger than a threshold value (0–280 μm was used in this study). One can visualize this 'shrink–wrap' function as placing a sphere inside the scaffold and observing if this sphere can reach the entire porous structure. The algorithm calculates how much of the porous structure is accessible to this sphere and it is defined as 'percentage of connective porosity.' The first calculation is done with a sphere diameter of 2 μm and continued stepwise until a diameter of 280 μm.

The algorithm calculates the interconnectivity as follows:

$$\text{Interconnectivity} = \frac{V - V_{\text{shrink-wrap}}}{V - V_{\text{m}}} \times 100\%, \quad (2)$$

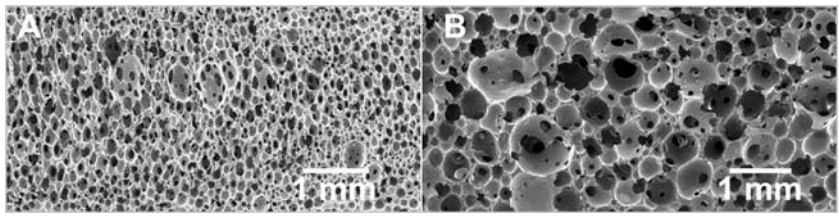


**Figure 3.** Pore morphology at 35% (a) and 55% (b) degree of weight reduction.

where $V$ is the total volume of VOI, $V_{\text{shrink–wrap}}$ the VOI volume after shrink–wrap processing, and $V_{\text{m}}$ the volume of scaffold material.

## Results and discussion

### *Influence of the weight reduction and gas content*

In this study, the gas content was varied from 1% to 6%; the degree of weight reduction was also varied from 35% to 65%. The injection speed, plasticizing temperature, plasticizing pressure, and mold temperature were fixed as 120 mm/s, 190°C, 170 bar and 25°C, respectively. SEM images (Figure 3) showed qualitatively differences of the pore structures. The porous diameter at 35% weight reduction (Figure 3(a)) was significantly smaller than the value at a higher degree of 55% (Figure 3(b)). The graphs for every degree of weight reduction showed the same tendency; increasing gas content led to a reduction in pore size (Figure 4(a)). The rise of gas content led to higher nucleus formation and consequently more pores. As a result, the mean pore size decreased because of the unchanged volume for the foam structure. The mean pore size dropped quickly for a gas content from 1% to 2%; the rate changed with higher content and reached a plateau at 6%. At the same gas content, the mean pore size also increased with the rise in weight reduction. At 1% of the gas content, the mean pore size increased from 230 to 864 µm with the rise of weight reduction from 35% to 65%; whereas, this change range of mean pore size was small at higher gas content of 6%, from 135 to 339 µm (Figure 4(a)). The change of cell density of the foamed sample agreed with the mean pore size change on the other side. The cell density by 35% weight reduction was increased from $1.4 \times 10^6$ to $7.5 \times 10^6$ per $\text{cm}^3$ for the gas content ranges from 1% to 6%. The other degrees of weight reduction showed also similar cell density curves.

Another important factor of pore morphology was the porosity which indicated the foaming degree of the foamed samples. The porosity changes were similar to the finding with the mean pore size. The rise of gas content led to an increase of porosity, which corresponded to the relevant rise of cell density. The porosity of 35% weight reduction had a range between 60% and 69% with rising gas content and the increase of weight reduction up to 65% shifted this porosity range to a higher value, between 73% and 79%, which means rising both gas content and

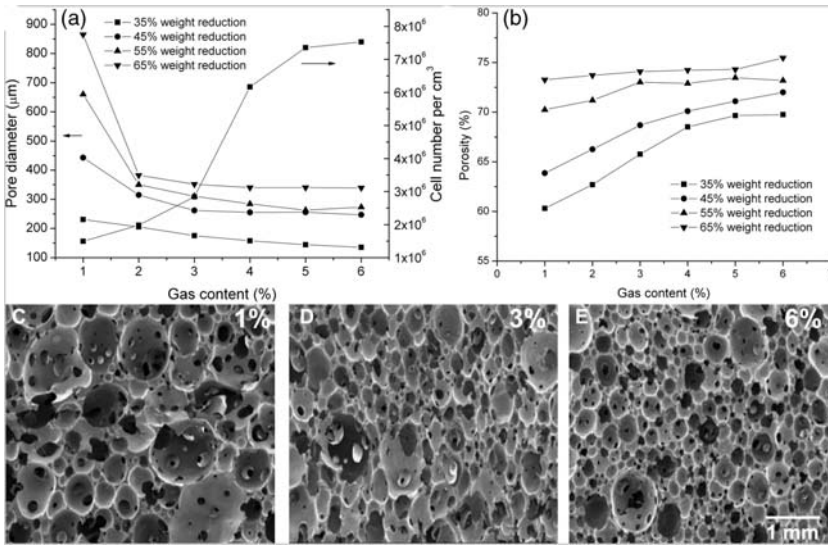


**Figure 4.** Pore diameters, cell densities (a), and porosities (b) of the foamed scaffolds at different gas contents and weight reductions (Every value was the average value from four different samples produced with the same parameters. The standard deviation was not drawn in the curve because of the disturbance of curve observation.) and SEM images of identical magnification with gas content 1% (c), 3% (d) and 6% (e).

weight reduction led to a higher porosity in the MuCell® process (Figure 4(b)). The SEM images in Figure 4(c)–(e) show the pore morphology at different gas contents (1%, 3% and 6%) with constant weight reduction of 55%. The change of pore morphology was obvious; with rise of the gas content, the pore size decreased obviously. The values of interconnection size, which means the window between two connective pores, in relation to the gas content and weight reduction are shown in Figure 5(a) and (b). Interconnections display the 'openness' of the porous structure and is a vital parameter for allowing cellular ingrowth.[44,45] The change in trend of the interconnection size was just as same as the mean pore size. Rising gas content led to a decrease of both mean pore size and interconnection size; for example, by 35% weight reduction, the range of interconnection pore size was between 108 and 40 μm. By higher weight reduction of 65%, the interconnection pore size changed from 131 μm to 52 μm by increasing the gas content from 1 to 6 wt.% (Figure 5(a)). Figure 5(b) shows the connective porosity depending on interconnection size of the foamed sample. The connective porosity compared with normally measured porosity means the porosity which consists of all the connective pores larger than the defined interconnective pore size. This value shows the interconnectivity of the foamed sample and was one of the most important characteristics of the porous structure. If the defined interconnection size was 0 μm, all the pores will be counted in the porosity, which means 100% measured porosity was effective. With rising of the defined interconnection size from 0 to 70 μm (interval 14 μm), the amount of

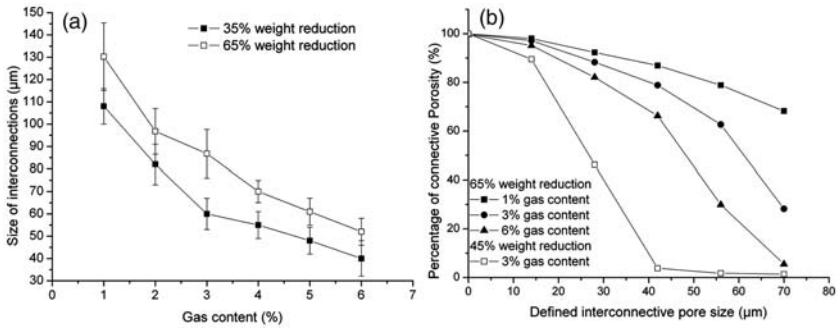


**Figure 5.** Size of interconnections (a) and interconnective porosities (b) in relation to gas content and weight reduction.

connective pores as well as the connective porosity decreased. By weight reduction of 65% and with 1% gas content, the relative porosity decreased from 100% to 68%, but with 6% gas content, this range was between 100% and 5.5%. Therefore, the increase of gas content can lead to not only a lower interconnectivity but also a rapid decrease of the interconnectivity of the foamed sample. Similarly, low weight reduction of 45% with gas content 3% means less free volume for the pore formation; therefore, the interconnectivity (from 100% to 1.5%) showed a faster plunge in comparison to the same gas content but a higher weight reduction of 65%, relative porosity from 100% to 28%.

## *Influence of the injection speed*

The injection speed of the process was the velocity at which the polymer–gas–solution was injected through the nozzle into the mold. According to the nucleation theory,[46–48] the main driving force of cell nucleation in MuCell® process was the pressure decrease at a very short time period. The injection speed of the polymer–gas–solution directly decides the pressure of the mixture at the point out of the nozzle as well as the pressure drop range; therefore, the effect of injection speed on the porous structure of the foamed part was expected. The range of injection speed in this study was 30–300 mm/s with an interval of 30 mm/s. The other fixed parameters were weight reduction (55%), gas content (2%), mold temperature (25°C), and plasticizing pressure and temperature (170 bar, 190°C). It was found (Figure 6(a)) that the mean pore size became smaller with rising the injection speed. This change can be attributed to more cell nucleation of the decrease in higher pressure induced by the higher injection speed. As a result, the smaller mean pore size and higher cell density was observed. In this case, the mean pore size decreased from 340 to 246 µm with the rise in injection speed from 30 to 300 mm/s, whereas the cell density increased from $5.8 \times 10^5$ to $1.6 \times 10^6$ per $cm^3$. Theoretically, this change in trend should be independent of the material used and also was observed by Kawashima et al.[35] when studying polystyrene (PS),

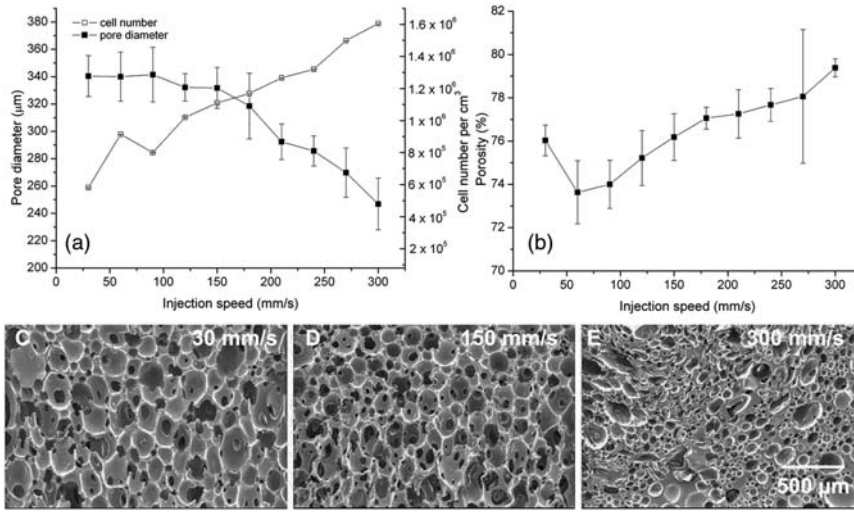


**Figure 6.** Pore diameters, cell densities (a), and porosities (b) of the foamed scaffolds at injection speeds and SEM images of pore morphology at 30 mm/s (c), 150 mm/s (d), and 300 mm/s (e), all with identical magnification.

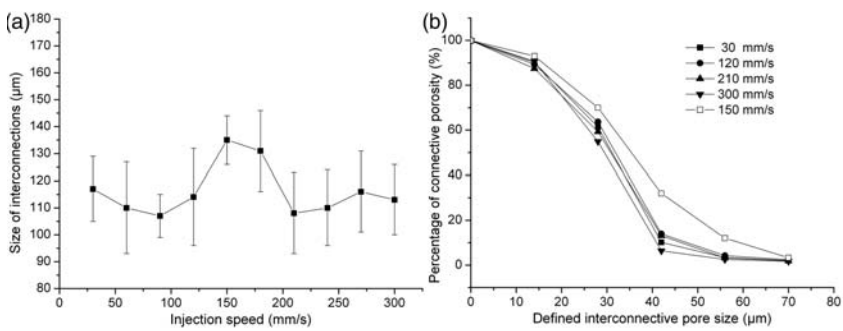


**Figure 7.** Size of interconnections (a) and interconnective porosities (b) in relation to the injection speed.

but nothing was found about other commercial materials such as polyethylene or polypropylene. The porosity at different injection speeds is illustrated in Figure 6(b). At an injection speed range from 30 to 60 mm/s, the porosity showed a slight drop from 76% to 73%, but after 60 mm/s, the porosity increased continuously from 73% to 79%. The findings from the microCT analysis can also be confirmed in the SEM images (Figure 6(c)–(e)). The size of the interconnection did not show a regular change (Figure 7(a)). A peak of 135 μm was found at the injection speed of 150 mm/s, whereas at speed ranges 30–120 and 210–300 mm/s, the size of the interconnections stayed in a small range 107–116 μm. No relevant

report was found about this phenomenon by other materials; so, the generality of this rule needs to be further researched. It was also observed from Figure 7(b) that injection speed change had nearly no effect on the connective porosity except at the speed of 150 mm/s. The curve of injection speed 150 mm/s showed a higher percentage of connective porosity at every defined interconnective pore size, which was consistent with the larger size of interconnection at 150 mm/s.

## *Influence of the plasticizing temperature*

The plasticizing temperature decided the solubility and solution speed of gas in the polymer melt; e.g., higher temperature induces possibly more homogeneous and faster gas dissolution in the polymer melt, which gave the possibility to change the morphology of the foamed part by varying the plasticizing temperature. The plasticizing temperature varied from 180°C to 210°C with an interval of 15°C. The fixed parameters were degree of weight reduction (55%), gas content (2%), injection speed (120 mm/s), plasticizing pressure (170 bar), and mold temperature (25°C). From the SEM images it is observed that with rising plasticizing temperature the pore diameter shows a profound decrease (Figure 8(d)–(f)). The qualitative changes of the mean pore size and cell density are shown in Figure 8(a). The mean pore size decreased slightly from 353 to 304 μm by temperature elevation from 180°C to 210°C, whereas the cell density increased quickly from $3.3 \times 10^5$ to $8.8 \times 10^5$ per $cm^3$. A similar result was also reported by producing soft rubber foams of poly(ethylene-co-vinyl acetate) using $CO_2$ as a gas foam agent in the expansion process.[49] The higher temperature led to a more homogenous distribution of gas in the polymer melt. Consequently, more pores were generated and decreased mean pore size and increased cell density were observed. The temperature-dependent porosity showed a slight increase from 68% to 71% corresponding to the reduction of mean size (Figure 8(b)). The interconnection size indicated a slight decrease from 129 to 113 μm. These small changes in porosity and interconnection size can be normally disregarded if compared with the results from the influences of weight reduction and gas content.

Despite the imperceptible changes of porosity and interconnection size at different plasticizing temperatures, the percentage of connective porosity showed different results (Figure 8(c)). At a low plasticizing temperature of 180°C, the connective porosity was significantly larger than at high temperatures of 195°C and 210°C. The foamed sample at a high plasticizing temperature had almost no connective porosity if the effective pores were defined as having an interconnective pore size larger than 42 μm, but at a temperature of 180°C, this connective porosity was even at 29.69% with an interconnective pore size of 70 μm.

## *Influence of the plasticizing pressure*

The plasticizing pressure was defined as the pressure at which the polymer was plasticized and gas was injected into the polymer melt. Changing this pressure

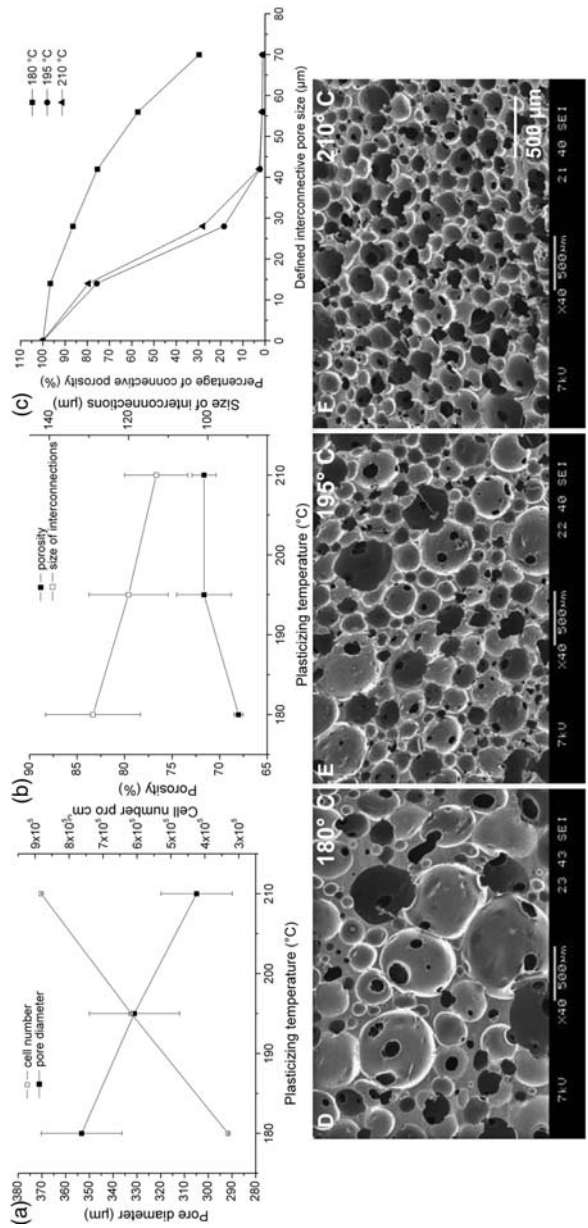


**Figure 8.** Pore diameters, cell densities (a), porosities and size of interconnections (b), and connective porosities (c) at different plasticizing temperatures and SEM pore morphology at plasticizing temperatures of 180°C (d), 195°C (e), and 210°C (f), all with identical magnification.

could affect the gas dissolution in polymer melt and result in the change of pore structure. The plasticizing pressure varied from 110 to 200 bar with an interval of 30 bar. The other parameters were degree of weight reduction (55%), gas content (2%), injection speed (120 mm/s), plasticizing temperature (190°C), and mold temperature (25°C). Quantitative curves of mean pore size, cell density, porosity, and size of connection are shown in Figure 9(a). The mean pore size decreased from 330 to 275 μm with changes in plasticizing pressure from 110 to 200 bar, corresponding to a cell density increase from $4.4 \times 105$ to $9.1 \times 105$ per $cm^2$. The visual effect can also be viewed in the SEM section at different plasticizing pressures (Figure 9(d)–(g)). This can be explained by the more homogeneous gas dissolution with higher degree induced by high pressure. Similar effect of pressure on the mean pore size and cell density has also been reported in literatures,[49–51] and its effect was believed to be linked to an improved dissolution behavior of gas in the polymer melt at elevated pressures. The porosity of the foamed sample at the different plasticizing pressures indicated a slight drop from 75% to 68% with plasticizing range up to 140 bar and remained nearly unchanged up to 200 bar (Figure 9(b)), despite a continuous increase in cell density. Concurrently, the interconnective pore size did not show a regular change, but just two plateaus of 116 and 86 μm. The porosity was more sensitive to the change in plasticizing pressure at the low area. The percentage of connective porosity in relation to the defined interconnective pore size (Figure 9(c)) showed a significant change with varying the plasticizing pressure. At 110 bar, the curve indicated a low interconnectivity. The connective porosity increased continuously with rise of the plasticizing pressure from 110 to 200 bar. This enabled the enhancement of interconnectivity through increasing the plasticizing pressure.

## *Influence of the mold temperature*

The mold temperature was the environment temperature at which the cell growth and cell stabilization take place. This temperature decided the change of viscosity of the injected polymer melt and consequently the cooling time of the polymer melt in the mold. Short cooling time could lead to an incomplete cell growth with a small cell size (<10°C). On the contrary, longer cooling time could also induce smaller cell sizes. This is due to the fact that the polymer structure collapses. Therefore, the mold temperature must be accurately adjusted to make sure that the polymer–gas–solution in the mold has a proper cooling time for the desired pore morphology. In this study, the mold temperature varied from 25°C to 85°C with interval of 20°C. The other parameters were degree of weight reduction (55%), gas content (2%), injection speed (120 mm/s), plasticizing temperature (190°C), and plasticizing pressure (170 bar).

Figure 10(a) shows quantitative changes of mean pore size and cell density at different mold temperatures. The mean pore size decreased from 371 to 240 μm by varying the mold temperature from 25°C to 85°C, whereas the cell density was just in the range $9.45 \times 10^5$ and $1.15 \times 10^6$ per $cm^3$. No regular change of cell density

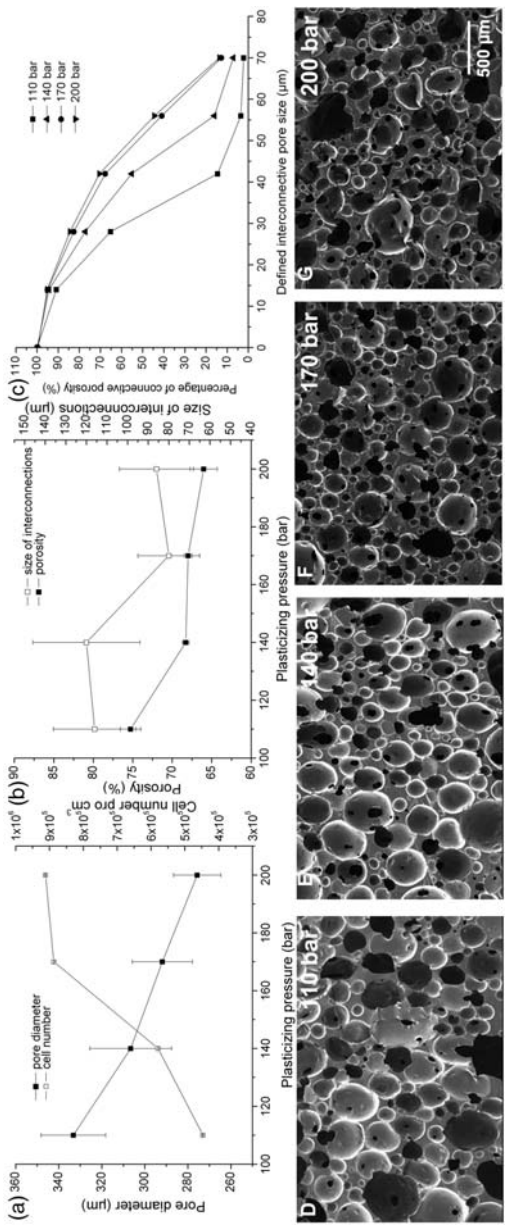


**Figure 9.** Pore sizes, cell densities (a), porosities and size of interconnections (b), and connective porosities (c) at different plasticizing pressures and SEM pore morphology at 110 bar (d), 140 bar (e), 170 bar (f), and 200 bar (g), all with identical magnification.

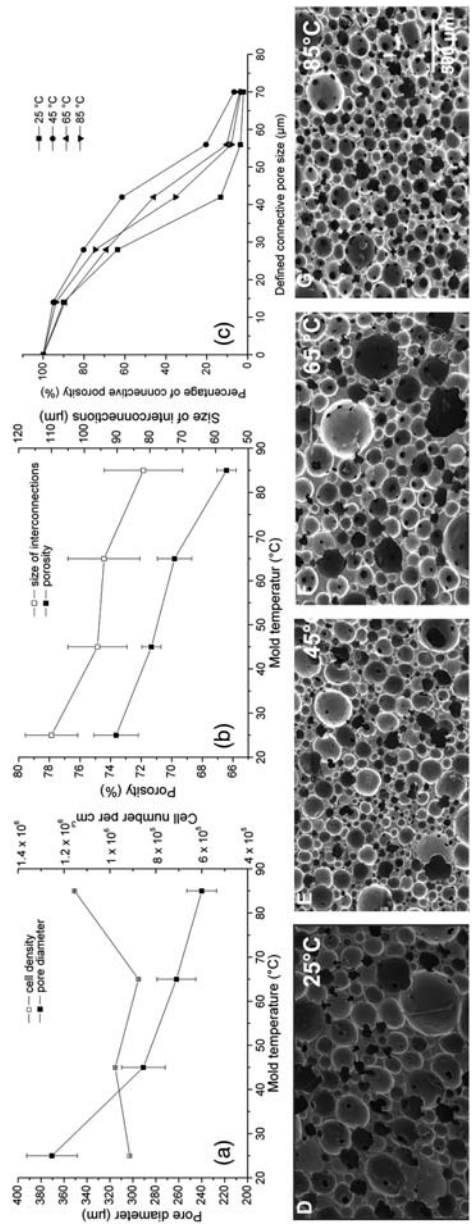


**Figure 10.** Pore sizes, cell densities (a), porosities and size of interconnections (b), and connective porosities depending on the defined interconnective pore size (c) at different mold temperatures And pore morphology at mold temperatures of 25° C (d), 45° C (e), 65° C (f), and 85° C (g), all with identical magnification.

**Table 2.** Average porosity and standard deviation

| Tested samples | Average porosity |
|---|---|
| Single batch ($n = 5$) | $71.4 \pm 4.9$ |
| Series of batches ($n = 6$) | $71.2 \pm 2.9\%$ |

**Table 3.** The relationships between process parameters and pore morphology

| Process parameters | Pore size | Porosity | Interconnective pore size |
|---|---|---|---|
| Gas content | ↓ | ↑ | ↓ |
| Weight reduction | ↑ | ↑ | ↑ |
| Injection speed | ↓ | ↑ | relationship not obvious |
| Plasticizing temperature | ↓ | ↑ | ↓ |
| Plasticizing pressure | ↓ | ↓ | relationship not obvious |
| Mold temperature | ↓ | ↓ | ↓ |

Notes: The arrow means the change in trend with increased value of each process parameter. Some process parameters such as gas content, weight reduction, and plasticizing temperature showed a more obvious influence on the pore morphology whereas some others had just a slight effect on the pore structure (arrows in bold indicate a strong increasing or decreasing effect and normal arrows a slight one).

was found. An increase of mean pore size with rising mold temperature was found by foaming PS.[35] But in the other case of foaming polyethylene terephthalate (PET) with different chemical structures, the reduction of mean pore size with increase of the mold temperature was also found,[50] although different processes were used in the foaming of PET. It can be consequently assumed that the influence of mold temperature on the pore morphology was rather material dependent, but further experiments need to be performed. Slices of the scaffold were also observed in SEM, where one can see the same behavior for the pore morphology for the different mold temperatures (Figure 10(d)–(g)). The porosity has slightly decreased from 73% to 66% as well as the size of interconnections, respectively, from 110 to 82 μm (Figure 10(b)), by varying the mold temperature from 25°C to 85°C. The porosity here was also in inverse proportion to the cell density on varying the plasticizing pressure. Figure 10(c) shows the interconnectivity of the foamed samples at different mold temperatures. The curve of 25°C indicated a worst interconnectivity despite the highest porosity and biggest mean pore size, but on the other hand, the best interconnectivity was found at the temperature of 45°C, not the highest temperature; so, no relation between the mold temperature and connective porosity was observed.

The standard deviations for the porosity of the samples were measured within one batch and on six different batches. The scaffolds were produced with the setting

of 55% weight reduction and 2% gas content. The standard deviation was found to be 4.9% for a single batch and 2.8% for six batches. The mean porosity varied from 71.4% to 71.2%, respectively (Table 2). The repeatability of the whole process was thus proven.

Table 3 briefly displays the overall influences of these key process parameters on the pore morphology of a polyurethane scaffold. The fat arrows in table 3 show the most important process parameters and how they govern the open porous structure.

## Conclusions

The main goal of this study was to produce an open porous scaffold through the MuCell® process and to determine the relationship between the resulting porous morphology and the processing parameters. This aim was fully achieved as an open porous structure with a porosity of 71% and proven interconnections could be made. The detailed relation between process parameter changes and pore morphology was hereby described. It was found that gas content and weight reduction were the prime influence factors of pore morphology in the MuCell® process. The gas content directly decided the amount of nucleus formation; the degree of weight reduction, which means, how many percentage of mold cavity was filled compared with compact injection, gave a space for the formation of a foamed structure. The higher gas content can lead to a larger foaming potential, but the gas solubility in the polymer melt had a limit; on the other side, without enough expandable volume for the foaming, the porous structure cannot form. Injection speed, plasticizing pressure, plasticizing temperature, and mold temperature were the second prime influence factors of pore morphology. It is believed that other open porous polymers would behave accordingly; however, the investigation of this hypothesis is out of scope for this study.

The pore size of the foamed scaffolds during the whole study ranged from 130 to 870 μm. The maximal porosity and interconnective pore size were 75% and 135 μm. It was proved that open porous scaffolds could be made on a large scale of using the MuCell® process, and that the pore morphology was controllable through varying the key processing parameters. Even though the foaming theory could be applied to describe the pore development, interaction of different parameters must be taken into account to fit the experimental data into the theory.

### Funding

The authors acknowledge the financial support provided by Bayerische Forschungsstiftung (grant no. AZ 639/05).

### References

1. Vacanti JP, Shieh SJ and Terada S. Tissue engineering auricular reconstruction: in vitro and in vivo studies. *Biomaterials* 2004; 25: 1545–1557.

2. Stock UA and Vacanti JP. Tissue engineering: current state and prospects. *Annu Rev Med* 2001; 52: 443–451.
3. Guldberg RE, Duvall CL, Peister A, Oest ME, Lin AS, Palmer AW, et al. 3D imaging of tissue integration with porous biomaterials. *Biomaterials* 2008; 29: 3757–3761.
4. Rucker M, Laschke MW, Junker D, Carvalho C, Schramm A, Mulhaupt R, et al. Angiogenic and inflammatory response to biodegradable scaffolds in dorsal skinfold chambers of mice. *Biomaterials* 2006; 27: 5027–5038.
5. Kidd KR, Dal Ponte DB, Kellar RS and Williams SK. A comparative evaluation of the tissue responses associated with polymeric implants in the rat and mouse. *J Biomed Mater Res* 2002; 59: 682–689.
6. Tienen TG, Heijkants RG, de Groot JH, Schouten AJ, Pennings AJ, Veth RP, et al. Meniscal replacement in dogs. Tissue regeneration in two different materials with similar properties. *J Biomed Mater Res B Appl Biomater* 2006; 76: 389–396.
7. Geffre CP, Margolis DS, Ruth JT, Deyoung DW, Tellis BC and Szivek JA. A novel biomimetic polymer scaffold design enhances bone ingrowth. *J Biomed Mater Res A* 2009; 91: 795–805.
8. Claro FA, Lima JR, Salgado MA and Gomes MF. Porous polyethylene for tissue engineering applications in diabetic rats treated with calcitonin: histomorphometric analysis. *Int J Oral Maxillofac Implants* 2005; 20: 211–219.
9. Laurencin CT, Attawia MA, Elgendy HE and Herbert KM. Tissue engineered bone-regeneration using degradable polymers: the formation of mineralized matrices. *Bone* 1996; 19: 93S–99S.
10. Mikos AG, Peter SJ, Miller MJ, Yasko AW and Yaszemski MJ. Polymer concepts in tissue engineering. *J Biomed Mater Res* 1998; 43: 422–427.
11. Thomson RC, Yaszemski MJ, Powers JM and Mikos AG. Fabrication of biodegradable polymer scaffolds to engineer trabecular bone. *J Biomater Sci Polym Ed* 1995; 7: 23–38.
12. Adhikari R, Gunatillake PA, Griffiths I, Tatai L, Wickramaratna M, Houshyar S, et al. Biodegradable injectable polyurethanes: synthesis and evaluation for orthopaedic applications. *Biomaterials* 2008; 29: 3762–3770.
13. Fassina L, Visai L, De Angelis MG, Benazzo F and Magenes G. Surface modification of a porous polyurethane through a culture of human osteoblasts and an electromagnetic bioreactor. *Technol Health Care* 2007; 15: 33–45.
14. Fassina L, Visai L, Benazzo F, Benedetti L, Calligaro A, De Angelis MG, et al. Effects of electromagnetic stimulation on calcified matrix production by SAOS-2 cells over a polyurethane porous scaffold. *Tissue Eng* 2006; 12: 1985–1999.
15. Fassina L, Visai L, Asti L, Benazzo F, Speziale P, Tanzi MC, et al. Calcified matrix production by SAOS-2 cells inside a polyurethane porous scaffold, using a perfusion bioreactor. *Tissue Eng* 2005; 11: 685–700.
16. Bertoldi S, Fare S, Ciapetti G and Tanzi MC. Polyurethane foams and Ca-P composites for bone tissue engineering. *J Appl Biomater Biom* 2007; 5: 195–199.
17. Aho AJ, Tirri T and Kukkonen J. Injectable bioactive glass/biodegradable polymer composite for bone and cartilage reconstruction: concept and experimental outcome with thermoplastic composites of poly(epsilon-caprolactone-co-d,l-lactide) and bioactive glass. *J Mater Sci Mater Med* 2004; 15: 1165–1173.
18. Daltona PD, Grafahrend D, Klinkhammer K, Kleeb D and Möllerb M. Electrospinning of polymernext term melts: phenomenological observations. *Polymer* 2007; 48: 6823–6833.

19. Maquet V, Boccaccini AR, Pravata L, Notingher I and Jérôme R. Preparation, characterization, and in vitro degradation of bioresorbable and bioactive composites based on Bioglass®-filled polylactide foams. *J Biomed Mater Res A* 2003; 66A: 335–346.
20. Rodriguez R, Estevez M, Vargas S, Gonzalez M, Salazar R and Pacheco F. Synthesis and characterization of HAp-based porous materials. *Mater Lett* 2009; 63: 1558–1561.
21. Haugen H, Will J, Fuchs W and Wintermantel E. A novel processing method for injection-molded polyether-urethane scaffolds. Part 1: Processing. *J Biomed Mater Res B Appl Biomater* 2006; 77B: 65–72.
22. Haugen H, Ried V, Brunner M, Will J and Wintermantel E. Water as foaming agent for open cell polyurethane structures. *J Mater Sci Mater Med* 2004; 15: 343–346.
23. Turng LS and Kramschuster A. An injection molding process for manufacturing highly porous and interconnected biodegradable polymer matrices for use as tissue engineering scaffolds. *J Biomed Mater Res B Appl Biomater* 2010; 92B: 366–376.
24. Leicher S, Will J, Haugen H and Wintermantel E. MuCell (R) technology for injection molding: a processing method for polyether-urethane scaffolds. *J Mater Sci* 2005; 40: 4613–4618.
25. [Anonymous] (2000). Ferromatik Milacron to convert 40 presses to MuCell process. *Mod Plast* 2000; 77: 11.
26. Toensmeier PA. Microcellular foam could increase appeal of nylon in underhood parts. *Plast Eng* 2006; 62: 10.
27. Bledzki AK, Rohleder M, Kirschling H and Chate A. Microcellular polycarbonate with improved notched impact strength produced by injection moulding with physical blowing agent. *Cell Polym* 2008; 27: 327–345.
28. Vanvuchelen J, Perugini C, Deweerdt M, Chen L and Burnham T. Microcellular PVC foam for thin wall profile. *J Cell Plast* 2000; 36: 148–152.
29. Dassow J. Foamed parts with excellent surface quality. *Kunstst-Plast Eur* 2003; 93: 25–27.
30. Rief B and Gundrum J. MuCell process: microcellular parts from the injection moulding machine. *Kunstst-Plast Eur* 2003; 93: 42–46.
31. Schonherr O. Physical foaming for cost effective injection moulding. *Kunstst-Plast Eur* 2003; 93: 22–28.
32. Hutmacher DW. Scaffold design and fabrication technologies for engineering tissues – state of the art and future perspectives. *J Biomater Sci Polym Ed* 2001; 12: 107–124.
33. Hutmacher DW. Scaffolds in tissue engineering bone and cartilage. *Biomaterials* 2000; 21: 2529–2543.
34. Wintermantel E and Ha S-W. *Medizintechnik*, 4th ed. Berlin: Springer Verlag, 2008.
35. Kawashima H and Shimbo M. Effect of key process variables on microstructure of injection molded microcellular polystyrene foams. *Cell Polym* 2003; 22: 175–190.
36. Okamoto KT. *Microcellular processing*. Munich: Carl Hanser Verlag, 2003.
37. Haugen H, Aigner J, Brunner M and Wintermantel E. A novel processing method for injection-molded polyether-urethane scaffolds. Part 2: Cellular interactions. *J Biomed Mater Res B Appl Biomater* 2006; 77B: 73–78.
38. Haugen H, Gerhardt LC, Will J and Wintermantel E. Biostability of polyether-urethane scaffolds: a comparison of two novel processing methods and the effect of higher gamma-irradiation dose. *J Biomed Mater Res B Appl Biomater* 2005; 73B: 229–237.
39. Haugen HJ.: Development of an implant to treat gastro-oesophageal reflux disease, PhD thesis. Technical University of Munich, 2004.

40. Haugen HJ, Brunner M, Pellikofer F, Aigner J, Will J and Wintermantel E. Effect of different gamma-irradiation doses on cytotoxicity and material properties of porous polyether-urethane polymer. *J Biomed Mater Res B Appl Biomater* 2007; 80B: 415–423.
41. Colton JS and Suh NP. The nucleation of microcellular thermoplastic foam with additives. Part 2: Experimental results and discussion. *Polym Eng Sci* 1987; 27: 463–499.
42. Lothe J and Pound GM. Reconsiderations of nucleation theory. *J Chem Phys* 1962; 36: 2080–2085.
43. Moore MJ, Jabbari E, Ritman EL, Lu LC, Currier BL, Windebank AJ, et al. Quantitative analysis of interconnectivity of porous biodegradable scaffolds with micro-computed tomography. *J Biomed Mater Res A* 2004; 71A: 258–267.
44. Lu JX, Flautre B, Anselme K, Hardouin P, Gallur A, Descamps M, et al. Role of interconnections in porous bioceramics on bone recolonization in vitro and in vivo. *J Mater Sci Mater Med* 1999; 10: 111–120.
45. Mastrogiacomo M, Scaglione S, Martinetti R, Dolcini L, Beltrame F, Cancedda R, et al. Role of scaffold internal structure on in vivo bone formation in macroporous calcium phosphate bioceramics. *Biomaterials* 2006; 27: 3230–3237.
46. Abraham FF. *Homogeneous nucleation*. New York/London: Academic Press, 1974.
47. Skripov VP. *Metastable liquids*. New York/London: Wiley, 1974.
48. Delale CF, Hruby J and Marsik F. Homogeneous bubble nucleation in liquids: the classical theory revisited. *J Chem Phys* 2003; 118: 792–806.
49. Jacobs MA, Kennere MF and Keurenties JTF. Foam processing of poly(ethylene-co-vinyl acetate) rubber using supercritical carbon dioxide. *Polymer* 2004; 45: 7539–7547.
50. Baldwin DF. A microcellular processing study of poly(ethylene terephthalate) in the amorphous and semicrystalline states. Part 2: cell growth and process design. *Polym Eng Sci* 1996; 36: 1446–1453.
51. Dai X, Liu Z, Wang Y, Yang G, Xu J and Han B. High damping property of microcellular polymer prepared by friendly environmental approach. *J Supercrit Fluid* 2005; 33: 259–267.